

# Uridine as a new scavenger for synchrotron-based structural biology techniques

Eva Crosas,<sup>a‡</sup> Albert Castellvi,<sup>a‡</sup> Isidro Crespo,<sup>a</sup> Daniel Fulla,<sup>a</sup>  
Fernando Gil-Ortiz,<sup>a</sup> Gustavo Fuertes,<sup>b</sup> Christina S. Kamma-Lorger,<sup>a</sup>  
Marc Malfois,<sup>a</sup> Miguel A. G. Aranda<sup>a</sup> and Jordi Juanhuix<sup>a\*</sup>

Received 16 June 2016

Accepted 17 November 2016

<sup>a</sup>ALBA Synchrotron, Carrer de la llum 2-26, 08290 Cerdanyola del Vallès, Barcelona, Spain, and

<sup>b</sup>EMBL, c/o DESY, Notkestrasse 85, 22607 Hamburg, Germany. \*Correspondence e-mail: juanhuix@cells.es

‡ These authors contributed equally to this work.

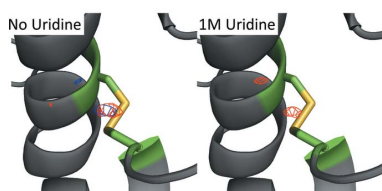
**Keywords:** radiation damage; reactive oxygen species; free radical scavenger; macromolecular crystallography methods; SAXS methods.

**Supporting information:** this article has supporting information at journals.iucr.org/s

Macromolecular crystallography (MX) and small-angle X-ray scattering (SAXS) studies on proteins at synchrotron light sources are commonly limited by the structural damage produced by the intense X-ray beam. Several effects, such as aggregation in protein solutions and global and site-specific damage in crystals, reduce the data quality or even introduce artefacts that can result in a biologically misleading structure. One strategy to reduce these negative effects is the inclusion of an additive in the buffer solution to act as a free radical scavenger. Here the properties of uridine as a scavenger for both SAXS and MX experiments on lysozyme at room temperature are examined. In MX experiments, upon addition of uridine at 1 M, the critical dose  $D_{1/2}$  is increased by a factor of  $\sim 1.7$ , a value similar to that obtained in the presence of the most commonly used scavengers such as ascorbate and sodium nitrate. Other figures of merit to assess radiation damage show a similar trend. In SAXS experiments, the scavenging effect of 40 mM uridine is similar to that of 5% v/v glycerol, and greater than 2 mM DTT and 1 mM ascorbic acid. In all cases, the protective effect of uridine is proportional to its concentration.

## 1. Introduction

Radiation damage is a well known limiting factor at third-generation synchrotron light sources for structural biology techniques such as small-angle X-ray scattering (SAXS) and macromolecular crystallography (MX). During the last decade, SAXS has arisen as a popular technique to obtain low-resolution envelopes of proteins in solution under nearly physiological conditions. Although samples for SAXS experiments are relatively uncomplicated to prepare, compared with crystallography, samples are required to be maintained in an aggregate-free, monodispersed form. A major factor that reduces data quality is the radiation damage caused by reactive oxygen species (ROS), such as hydroxyl ( $\text{OH}^\bullet$ ) and hydroperoxyl ( $\text{HO}_2^\bullet$ ) radicals, hydrogen radical ( $\text{H}^\bullet$ ) and solvated electrons which are generated by the radiolysis of water in the buffer solution (Garrison, 1987; Maleknia *et al.*, 2001) during data collection. These radicals rapidly react with the polypeptide chain (at a rate of  $10^9$ – $10^{10} \text{ M}^{-1} \text{ s}^{-1}$ ), leading to aggregation of the protein (Kuwamoto *et al.*, 2004; Garrison, 1987). The amino acids most sensitive to hydroxyl radical attack are Cys and Met, followed by the aromatic amino acids (Phe, Tyr, Trp) and then Pro, His and Leu. Regions more exposed to the solvent are more susceptible to hydroxyl radical attack (Maleknia *et al.*, 2001). Metal centres are also severely affected by radiation damage, suffering reduction upon exposure to X-rays. Aggregation,



which is the most evident effect observed in solutions, mainly affects SAXS data obtained at very small angles (low  $q$  or Guinier region), preventing size and shape determination of the protein. The scattering curve can also be affected at wide angles (Fischetti *et al.*, 2003), limiting the structural detail that can be obtained.

Data quality in MX experiments is also limited by radiation-induced disorder and structural damage. The excellent reviews in the literature (Murray *et al.*, 2005; Holton, 2009; Garman, 2010; Garman & Weik, 2011) show that damage can appear at a local or a global scale. Local radiation damage is revealed by the reduction of metallo-centers, the elongation and subsequent breaking of disulfide bonds, decarboxylation of aspartates and glutamates, cleavage of carbon–sulfur bonds in methionines and the breaking of covalent bonds to metals. Atomic  $B$ -factors also increase with absorbed dose (Gerstel *et al.*, 2015). Global radiation damage is apparent as a loss of resolution of the diffraction data, an increase of both the  $B$ -factor derived from the Wilson plot (Kmetko *et al.*, 2006) and that from the refinement of the structure (Gerstel *et al.*, 2015), and an increase of  $R_{\text{meas}}$  (Rajendran *et al.*, 2011) and  $R_{\text{damage}}$  (Diederichs, 2006). MX data collections at room temperature are largely limited by global radiation damage effects, whereas data collections at cryogenic temperatures are also affected, at higher doses, by specific radiation damage effects.

Proteins in solution are much more sensitive to X-ray irradiation than crystalline samples if only global damage is considered. While lysozyme solutions measured by SAXS show radiation-induced aggregation above absorbed doses of  $\sim 400$  Gy, or  $\sim 1$  kGy in the presence of glycerol (Kuwamoto *et al.*, 2004), lysozyme crystals used in MX experiments can tolerate absorbed doses of  $\sim 1$  MGy at room temperature (Barker *et al.*, 2009) before noticeable global damage effects become apparent. In either case, however, tolerated doses are usually smaller than the dose required to collect optimal data sets. Similar strategies are used in both techniques to limit the radiation damage of the samples. The most common strategy in MX, albeit insufficient or applicable in many cases, is the use of a cryogenic nitrogen gas stream to cool the sample to 100 K. The use of cryogenic temperatures has recently been applied to SAXS (Meisburger *et al.*, 2013). The cryo-SAXS method cryocools small volumes of sample, from  $\sim 20$  nL to  $\sim 1$   $\mu\text{L}$ , to 100 K, allowing the proteins and nucleic acids to withstand doses up to 100–300 kGy. Other strategies for both techniques include attenuating or defocusing the X-ray beam (Hura *et al.*, 2009; Schulze-Briese *et al.*, 2005), flowing the sample continuously (Barty *et al.*, 2012; Pernot *et al.*, 2013; Martel *et al.*, 2012; Nielsen *et al.*, 2012) or translating the sample through the beam (Hong & Hao, 2009; Flot *et al.*, 2010). Other approaches in SAXS include cooling the sample down to 4–10°C, which can be achieved with temperature-controlled cells coupled to automated collection systems (Hura *et al.*, 2009; Pernot *et al.*, 2013; Round *et al.*, 2015; Blanchet *et al.*, 2015), or reducing the exposure times (Fischetti *et al.*, 2003; Pernot *et al.*, 2013). However, beam defocusing or attenuation is used at the price of decreasing the signal-to-noise ratio, and flow or translation approaches

consume more sample. A further, complementary, strategy to limit radiation damage is the addition of ROS scavengers to the buffer solution. In SAXS experiments these additives include reducing agents such as dithiothreitol (DTT) or ascorbic acid (Grishaev, 2012; Jacques & Trehwella, 2010) which act as scavengers against ROS, or sugars such as glycerol, which reduce protein–protein interactions and react with the hydroxyl radicals and electrons created by X-ray radiation (Kuwamoto *et al.*, 2004). In MX experiments, the most commonly used scavengers are ascorbate and sodium nitrate (Barker *et al.*, 2009; De La Mora *et al.*, 2011). An extensive review of the use of scavengers in MX experiments is given by Allan *et al.* (2013).

Many compounds are described as having antioxidant properties, counteracting the effects of ROS on biological macromolecules. Interestingly, uridine, the ribonucleoside of the pyrimidine base uracil and one of the four standard nucleosides which constitute RNA, is found at high concentrations in the cytosol of *D. radiodurans* (Daly *et al.*, 2010), together with other bases, metabolites and peptides. This extremophile bacterium can withstand ionizing radiation up to 12 kGy although its DNA is as sensitive to ROS attack as that of other organisms which cannot withstand 12 kGy without damage (Daly *et al.*, 2010). The key factor in *D. radiodurans* ability to survive under extreme levels of irradiation is the persistence of a functional DNA repair system due to the presence of a collection of compounds in the cytosol (Daly *et al.*, 2010; Daly, 2012; Slade & Radman, 2011). Uridine reacts with solvated electrons and with hydroxyl and hydrogen radicals (Greenstock *et al.*, 1969). In combination with manganese and orthophosphate, uridine contributes to protecting the proteome, and in particular the DNA repair enzymes against exposure to high levels of radiation (Daly *et al.*, 2010). However, in spite of the known scavenging properties of uridine against radicals, to the best of our knowledge this compound has never been studied as a potential scavenger for SAXS or MX experiments.

Here we present a study of the properties of uridine as a scavenger to mitigate the radiation damage of lysozyme in SAXS and room-temperature MX experiments. For SAXS, we compare the performance of uridine with that of other well known compounds used to reduce radiation-induced aggregation such as DTT, glycerol and ascorbic acid. For MX, we show that the scavenging properties of uridine are similar to, and in some cases better than, those of ascorbate and sodium nitrate.

## 2. Materials and methods

### 2.1. Sample preparation

Chicken egg-white lysozyme (cEWL) was obtained from Sigma-Aldrich (L6876). The protein concentration in the corresponding buffer was determined by measuring the absorbance at 280 nm using an extinction coefficient of  $2.64 \text{ ml mg}^{-1} \text{ cm}^{-1}$ . Crystals for the MX experiments were grown according to the method given in De la Mora *et al.*

(2011) at different concentrations of lysozyme ranging between 50 mg ml<sup>-1</sup> and 80 mg ml<sup>-1</sup>. The mother liquor (100 mM sodium acetate, 10% sodium chloride at pH 4.7) does not have any scavenging properties. Only crystals with a size of around 100 × 100 × 50 µm were harvested for use in the experiments (see Table S1 of the supporting information for sizes of the individual crystals). The crystals of lysozyme used for diffraction at room temperature with uridine were prepared by soaking them in mother liquor containing three different concentrations of uridine (200 mM, 500 mM and 1 M). The uridine solutions replaced the corresponding amount of water in the mother liquor. The soaking time, which was not found to affect the outcome of initial test experiments, was varied from a few seconds to a few minutes. Crystals were introduced inside a polyimide capillary of 1 mm internal diameter (Goodfellow, IM307100) with the aid of a pipette. The crystals were adhered to the tube wall by removing the excess solution around them. Sample dehydration was prevented by keeping some solution around the crystal and by a solution reservoir pipetted near the crystal. The capillary was mounted on a SPINE magnetic cap compatible with the diffractometer. The crystals used for diffraction at 100 K were prepared as above with 500 mM and 1 M of uridine and with the addition of 25% (v/v) ethylene glycol as a cryoprotectant in the soaking solution.

cEWL is a well characterized protein used as a standard for molecular weight determination in solution scattering (Hammel *et al.*, 2002). cEWL solution for SAXS experiments was prepared at 8 mg ml<sup>-1</sup> in 40 mM sodium acetate, pH 3.8, 150 mM NaCl. The additives were freshly prepared as 10× stock solutions in 40 mM sodium acetate, pH 3.8, 150 mM NaCl. The additives were ten-fold diluted from the corresponding stocks in order to obtain the following final concentrations in the samples: 2 mM DTT, 5% v/v (679 mM) glycerol, 1 mM ascorbic acid, and 5, 10, 15, 20, 40 and 100 mM uridine. cEWL solutions without any additive were also prepared as a control. The final concentration of cEWL after the addition of the different compounds was 7.2 mg ml<sup>-1</sup>. The solutions were housed in a 1.8 mm quartz capillary (1.7 mm internal diameter, cell wall thickness 50 µm) held at 283 K under vacuum.

## 2.2. Data collection

Diffraction data collections at room temperature and at 100 K were performed at the BL13-XALOC beamline at the ALBA synchrotron (Juanhuix *et al.*, 2014) using a Pilatus 6M photon-counting detector (DECTRIS, Baden, Switzerland). The profile of the beam was Gaussian-shaped and was set at 12.661 keV photon energy ( $\lambda = 0.979$  Å). The sample–detector distance was adjusted to collect the data sets at a resolution of 1.4 Å and 1.1 Å for experiments at room temperature and at 100 K, respectively.

Eleven crystals soaked at different uridine concentrations (four crystals without, four 200 mM and three 500 mM uridine) were irradiated at room temperature at an absorbed dose rate of 13.8 kGy s<sup>-1</sup> (Table S1 of the supporting infor-

mation). Seven crystals (four crystals without uridine, three soaked at 1 M of uridine) were irradiated at room temperature at an absorbed dose rate of 20.0 kGy s<sup>-1</sup>. Finally, seven more crystals (three crystals without uridine, one soaked at 500 mM and three soaked at 1 M uridine) were irradiated at 100 K at a dose rate of 90 kGy s<sup>-1</sup>. The flux to calculate the dose was measured using a calibrated PIN Si diode at the sample position. The beam profile had a Gaussian shape and was defocused to a FWHM dimension of 86–100 µm (h) × 78–85 µm (v) as measured by a Ce:YAG fluorescent screen at the sample position. Complete data sets of 90 images were collected with an angle increment per image of 1°. The crystals at 100 K were ‘burned’ between data sets with an absorbed dose of 1230 kGy at a dose rate of 205.2 kGy s<sup>-1</sup>. The crystals were rotated by 90° during the ‘burns’. Burns were not performed for crystals at room temperature. For a given crystal, the successive data sets with increasing dose were collected starting from the same initial angle. The space group for all crystals was  $P4_32_12$ . All crystals had cell dimensions differing by less than 1 Å from those of the crystals without uridine at room temperature, that is,  $a = b = 79.2$  Å and  $c = 37.9$  Å (see Tables S2 and S3 of the supporting information).

SAXS profiles from lysozyme solutions were recorded at the EMBL P12 BioSAXS beamline at PETRA III (DESY, Hamburg, Germany) (Blanchet *et al.*, 2015) using a Pilatus 2M detector placed 3 m from the sample. The beam at the sample position had a flux of  $1.4 \times 10^{12}$  photons s<sup>-1</sup> at 10 keV photon energy ( $\lambda = 0.124$  nm) and a dimension of 500 × 250 µm (h × v, full beam). Multiple frames of 0.035 s exposure time at a dose rate of 5.4 kGy s<sup>-1</sup> were collected by using the EMBL automatic sample changer (Round *et al.*, 2015) with automated sample delivery and static sample data collection (hereafter called static mode). As a control, SAXS data for lysozyme without any additive and 0.045 s exposure time were collected by using continuous-flow automated sample delivery and data collection, *i.e.* the sample was flowing while exposed to the beam (hereafter flow mode). No attenuation was used.

## 2.3. Absorbed dose calculation

The dose,  $D$ , absorbed by the sample in SAXS experiments was calculated using Lambert’s law,

$$D = \frac{FEt}{m} \exp(-\mu\rho d), \quad (1)$$

where  $F$  is the incoming photon flux,  $E$  is the photon energy,  $t$  is the accumulated exposure time and  $m$  is the mass of the irradiated sample. In the absorption coefficient  $\exp(-\mu\rho d)$ ,  $\mu$  is the mass attenuation factor and  $\rho$  and  $d$  are the density and the thickness of the sample, respectively. For SAXS experiments the absorption coefficient was calculated taking into account the absorption of water and the thickness of the quartz capillary wall. The transmission of the sample was calculated using the Center for X-ray Optics server ([http://henke.lbl.gov/optical\\_constants/filter2.html](http://henke.lbl.gov/optical_constants/filter2.html); Henke *et al.*, 1993).

The average dose-exposed region (AD-ER) doses for the MX experiments were calculated with *RADDOSE-3D* (Zeldin

*et al.*, 2013). The crystal is assumed to have a cubic shape with dimensions measured by the on-line microscope of the beamline.

## 2.4. MX data processing

All datasets at room temperature in MX experiments were indexed and integrated between 50 Å and 2 Å using *XDS* (Kabsch, 2010). Data statistics for each dataset were extracted from the output files generated by *XDS*. The values of the relative diffraction intensity  $I/I_1$  and the *R*-damage factor  $R_d$  (Diederichs, 2006) were extracted from *XDSSTAT*. Data sets were scaled and structure factors generated using *AIMLESS* (Evans, 2006) and *TRUNCATE* (French & Wilson, 1978), respectively. Molecular replacement was not necessary since the initial Protein Data Bank (PDB) model used for lysozyme (1bwh) (Dong *et al.*, 1999) has the same space group and similar unit-cell dimensions as our data. The first refinement of the structure was performed *via* rigid-body minimization followed by restrained refinement using *REFMAC5* (Murshudov *et al.*, 1997). Subsequently, preliminary structures were iteratively refined through manual adjustment using *COOT* (Emsley *et al.*, 2010) (according to the allowed values in the Ramachandran plot, with a good fit in  $2F_o - F_c$  maps and with no significant peaks in  $F_o - F_c$  maps), and then through restrained refinement, until the crystallographic *R*-value and  $R_{\text{free}}$  were as low as achievable. Water molecules were added and replaced using *REFMAC5*. The refinement was completed when  $R_{\text{work}} < 0.20$  and  $R_{\text{free}} < 0.25$ . All the data sets from the same crystal were Wilson scaled together *via* *SCALEIT* (Howell & Smith, 1992). Difference Fourier maps ( $F_{\text{obs},n} - F_{\text{calc},1}$ ,  $\alpha_{\text{calc},1}$ ) were calculated between each dataset *n* and the initial data set using the phases of the fresh, not previously irradiated, data set  $\alpha_{\text{calc},1}$ , as described by Southworth-Davies *et al.* (2007). Other than *XDS*, all programs mentioned here belong to the *CCP4* programming suite (Winn *et al.*, 2011). Data sets collected at 100 K were integrated between 50 Å and 1.7 Å, and processed using the same protocol.

## 2.5. SAXS data processing

For globular proteins in solution, the radius of gyration  $R_g$  is a parameter highly sensitive to changes in the size of the particles in solution due to radiation damage (Kuwamoto *et al.*, 2004; Jeffries *et al.*, 2015).  $R_g$  in SAXS experiments was determined by using the Guinier approximation (Guinier, 1939), as implemented in the *PRIMUS* software (Konarev *et al.*, 2003), included in the *ATSAS* package (Petoukhov *et al.*, 2012). The relative increase of the radius of gyration with respect to the initial value in the first data frame,  $R_g/R_{g0}$ , was plotted against the absorbed dose. The critical dose where radiation-induced aggregation occurs was defined as the absorbed dose where  $R_g/R_{g0}$  increases at most by 10%.

The similarity between frames was assessed using the correlation map (*CorMap*) test (Franke *et al.*, 2015). The maximum particle dimension  $D_{\text{max}}$  and the pair-distance distribution function  $P(r)$  were determined with *GNOM*

(Svergun, 1992). The theoretical scattering profile of lysozyme was determined with *CRY SOL* (Svergun *et al.*, 1995) using the lysozyme crystal structure PDB ID 4n8z (Yin *et al.*, 2014). *Ab initio* modelling was performed by running *DAMMIF* (Franke & Svergun, 2009) 20 times in slow mode without imposing symmetry. Superposition of the low-resolution SAXS model onto the high-resolution MX structure was performed by using *SUPCOMB* (Kozin & Svergun, 2001) and visualized with *PyMOL* (The PyMOL Molecular Graphics System, Version 1.7, Schrödinger LLC).

## 3. Results

### 3.1. MX results

The radiation damage suffered by crystals in MX experiments can be evaluated on a global and local/specific scale. Global radiation damage is characterized here by using three metrics already mentioned: the dose,  $D_{1/2}$ , required to reduce the mean intensity of all reflections in a data set to half of the value of the first data set; the damage *R*-factor per image,  $R_d$ , as defined by Diederichs (2006); and the coefficient of sensitivity to absorbed dose,  $S_{\text{AD}} \equiv 8\pi^2(\Delta B/\Delta D)$  (Kmetko *et al.*, 2006, 2011), where the ratio  $\Delta B/\Delta D$  quantifies the increase of the mean *B*-factor induced by an additional dose. The experiments performed at 100 K show no scavenging effect of uridine in lysozyme crystals (data shown in Fig. S1 and Table S1 in the supporting information). Therefore, all results reported hereinafter are for measurements made at room temperature. All the metrics indicate an evolution of the crystal damage with dose that depends on the concentration of the uridine, as shown in Fig. 1. The protective effect of uridine increases with increasing concentration for all metrics. The scavenging effect of uridine at a given dose *D* is quantified *via* the enhancement factors defined as the ratio of the metrics calculated with and without uridine:  $D_{1/2,U}/D_{1/2,0}$ ,  $R_{d,U}/R_{d,0}$  at 1 MGy and  $S_{\text{AD,U}}/S_{\text{AD,0}}$  (Table 1, particular statistics for individual crystals are shown in Table S1 of the supporting information). Three other metrics to evaluate the radiation damage effects and the scavenging properties of uridine were tested but disregarded. The increment of the normalized  $R_{\text{merge}}$  and the normalized mosaicity with absorbed dose show consistent trends compared with other metrics, but the errors are too high to provide reliable values. The relative expansion of the unit-cell parameters is inconsistent as it does not show a defined pattern for all crystals under the same conditions, as has been reported in previous studies. The global radiation damage suffered by the crystals at room temperature not soaked with uridine does not show a dependence on dose rate, in agreement with results reported by Kmetko *et al.* (2011) and Warkentin *et al.* (2012), except for at high doses (above 1.2 MGy approximately), where all significant metrics in Fig. 1 indicate a slower structural damage at higher rates (20 kGy s<sup>-1</sup>, light grey points) compared with lower rates (13.8 kGy s<sup>-1</sup>, orange points).

Specific radiation damage was assessed using the difference Fourier maps calculated between the first data set and the

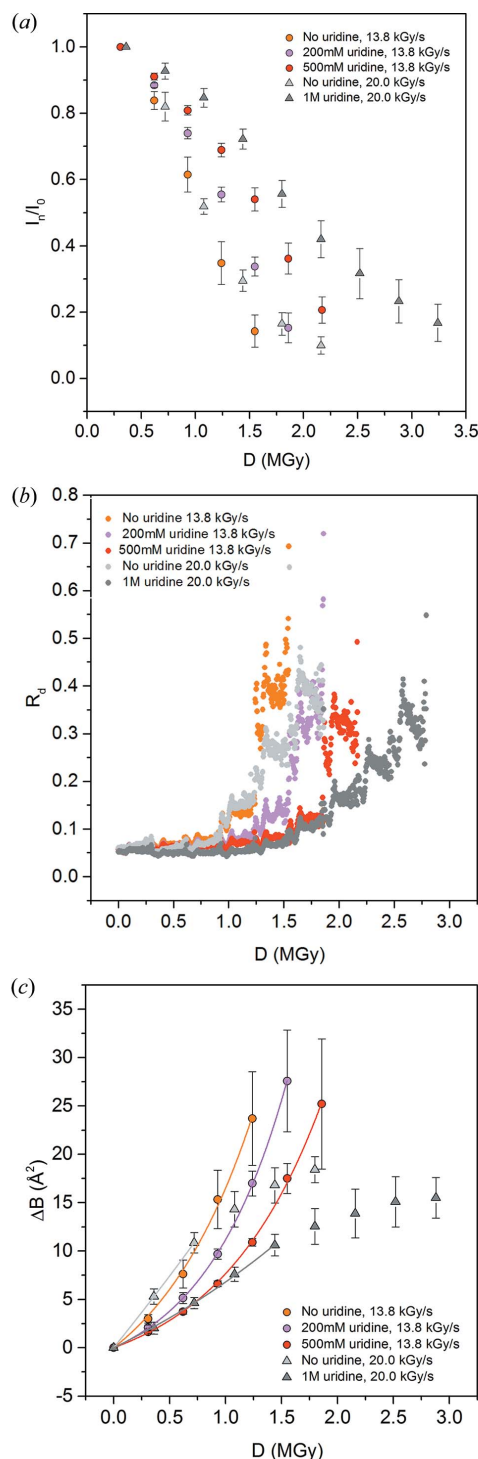


**Figure 1**

Evolution of radiation damage with absorbed dose on lysozyme crystals at room temperature monitored using different metrics. The dose  $D$  is defined as the total absorbed energy divided by the mass of the region of the crystal receiving nonzero dose (AD-ER), as defined by Zeldin *et al.* (2013). Crystals were soaked at different uridine concentrations, from zero to 1  $M$ , and diffraction data recorded at two different dose rates. (a) Decay of the mean normalized intensity  $I/I_1$ , calculated in the 50–2 Å resolution range. (b) Decay of the  $R$ -factor  $R_d$  with dose.  $R_d$  is calculated in the 50–2 Å resolution range. For clarity, error bars are not shown (data with error bars are plotted in Fig. S2 of the supporting information). (c) Evolution of  $\Delta B$  as a function of dose. Lines show the fits of the experimental data using an exponential model  $\Delta B = B_0[\exp(k\Delta D) - 1]$ . Results of the fits are shown in Table 1.

**Table 1**

Radiation damage metrics (top) and derived enhancement factors (below) for uridine in MX experiments in lysozyme crystals without, with 200 mM, with 500 mM and 1  $M$  of uridine.

$R_{d,U}$  factors are calculated at 1 MGy dose.  $\Delta B/\Delta D$  and  $S_{AD}$  values are calculated using the approximation  $\Delta B = B_0[\exp(k\Delta D) - 1] \approx B_0k\Delta D$  (valid at low doses).

Sample, dose rate	$D_{1/2}$ (MGy)	$R_{d,U}$	$\Delta B/\Delta D$ ( $S_{AD}$ ) (Å <sup>2</sup> MGy <sup>-1</sup> )
No uridine, 13.8 kGy s <sup>-1</sup>	1.06	0.120	9.07 (0.11)
No uridine, 20.0 kGy s <sup>-1</sup>	1.11	0.127	15.07 (0.19)
200 mM uridine, 13.8 kGy s <sup>-1</sup>	1.32	0.072	5.32 (0.07)
500 mM uridine, 13.8 kGy s <sup>-1</sup>	1.62	0.065	4.26 (0.05)
1000 mM uridine, 20.0 kGy s <sup>-1</sup>	1.95	0.049	5.63 (0.07)

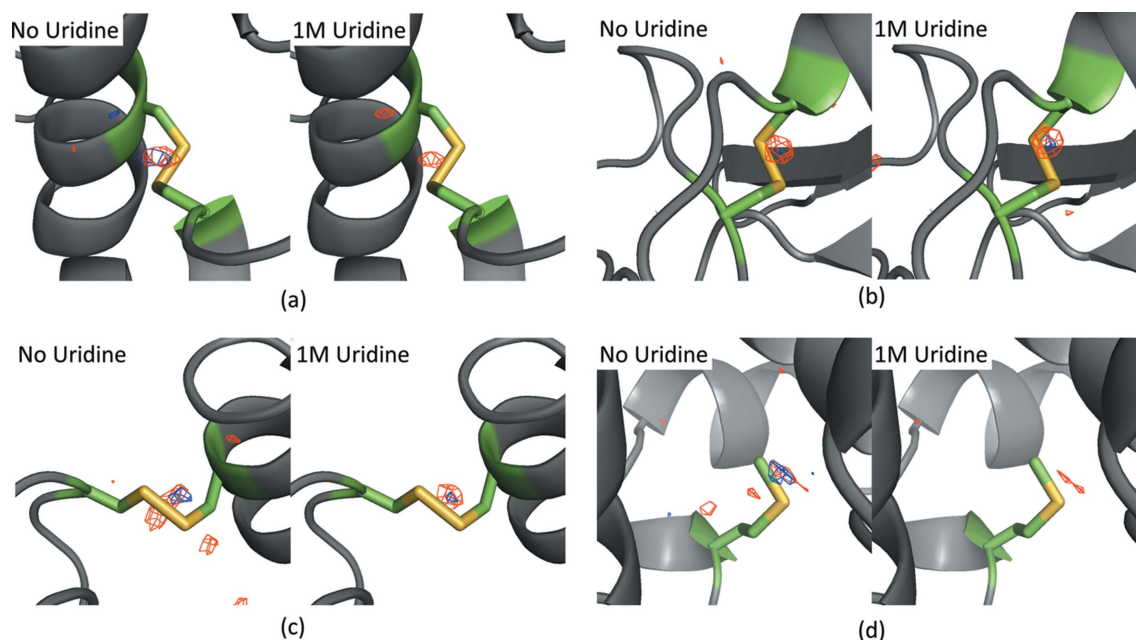
  

	$D_{1/2,U}/D_{1/2,0}$	$R_{d,U}/R_{d,0}$	$S_{AD,U}/S_{AD,0}$
200 mM uridine versus no uridine, 13.8 MGy s <sup>-1</sup>	1.24	0.59	0.58
500 mM uridine versus no uridine, 13.8 MGy s <sup>-1</sup>	1.52	0.55	0.47
1000 mM uridine versus no uridine, 20.0 MGy s <sup>-1</sup>	1.76	0.38	0.37

second and third data sets, ( $F_{obs,2} - F_{obs,1}$ ,  $\alpha_{calc,1}$ ) and ( $F_{obs,3} - F_{obs,1}$ ,  $\alpha_{calc,1}$ ), respectively, for the non-soaked crystals (PDB codes 519j, 51a5 and 51a8 for structures derived from the first, second and third data set, respectively) and for the crystals soaked at 1  $M$  uridine (PDB codes 51af, 51ag and 51an) (crystals 12 and 16, Table S2 of the supporting information). Each data set absorbed a dose of 0.36 MGy, and all were collected at a dose rate of 20 kGy s<sup>-1</sup>. The ( $F_{obs,3} - F_{obs,1}$ ,  $\alpha_{calc,1}$ ) maps of both crystals show significant peaks for Cys30–Cys115, Cys64–Cys80, Cys76–Cys94 disulfide bonds and Met105 (Fig. 2), but not for Cys6–Cys127 (data not shown). Beyond  $-4\sigma$  no significant peaks are observed for ( $F_{obs,3} - F_{obs,1}$ ,  $\alpha_{calc,1}$ ) maps. The  $2F_o - F_c$  and  $F_o - F_c$  maps of the crystals soaked at 1  $M$  uridine do not reveal the presence of ordered uridine in the crystallographic structure.

### 3.2. SAXS results

The performance of uridine as a compound to limit radiation damage on solutions of lysozyme is compared with that of DTT, ascorbic acid and glycerol, which are well known additives used for that purpose in SAXS experiments, by using the change in the radius of gyration  $R_g$  with the absorbed dose. The ratio of  $R_g$  at a given dose with respect to that of the first data frame,  $R_g/R_{g0}$ , is plotted against the accumulated dose for lysozyme in solution at concentrations of 5, 10, 15, 20, 40 and 100 mM uridine (Fig. 3). The critical dose was used to quantify the sensitivity to radiation for all these samples and was determined by using two different metrics. For the first metric, the critical dose is defined as the accumulated dose for which  $R_g/R_{g0}$  increases by a maximum of 10%. The critical dose for the second metric, as defined by Jeffries *et al.* (2015), is the dose required to induce an increment of 0.1 nm in the pseudo-radius of gyration,  $\Delta R_g^{ps}$ , relative to the initial data frame (Fig. 4). The metrics for solutions containing 2 mM DTT, 5%  $v/v$  glycerol and 1 mM ascorbic acid are also plotted



**Figure 2** Comparison of the  $(F_{\text{obs},2} - F_{\text{obs},1}, \alpha_{\text{calc},1})$  (blue) and  $(F_{\text{obs},3} - F_{\text{obs},1}, \alpha_{\text{calc},1})$  (red) maps between a crystal without uridine (left figures) and a crystal with 1 M of uridine (right figures) contoured at  $-4\sigma$ . (a) Cys30–Cys115. (b) Cys64–Cys80. (c) Cys76–Cys94. (d) Met105. Crystals used are 12 (no uridine) and 16 (1 M of uridine in solution). Data were collected at room temperature. See Table S2 for diffraction statistics.

for comparison, as these are additives at concentrations commonly used in SAXS experiments to limit radiation damage (Svergun *et al.*, 2013; Jeffries *et al.*, 2015). A solution containing no additives was also measured as a control. These indicators are consistent and show that sensitivity is significantly affected by the presence and concentration of the additives. From high to low, sensitivities of proteins in solution are: control > 1 mM ascorbic acid > 5 mM uridine > 2 mM DTT > 10 mM uridine > 15 mM uridine > 20 mM uridine >

5% v/v glycerol > 40 mM uridine > 100 mM uridine. As expected, critical doses for lysozyme containing additives are higher than for the negative control. More radiation-sensitive samples have a steeper slope of  $\Delta R_g^{\text{ps}}$  and  $R_g/R_{g0}$  for a given absorbed dose. The critical dose increases linearly with the concentration of uridine. According to the calculated critical doses for lysozyme in solution (Fig. 4), the scavenging effect of 2 mM DTT or 1 mM ascorbic acid is close to that of 5 mM uridine, whereas the scavenging effect of 5% v/v glycerol is between that of 20 and 40 mM uridine.

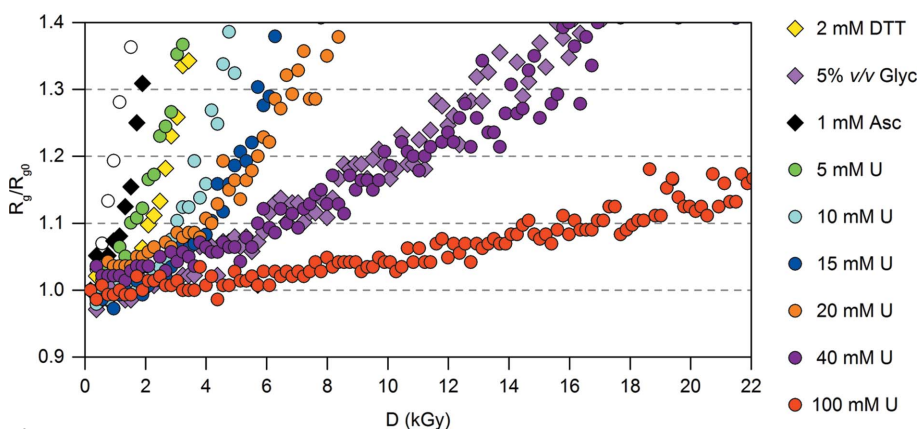


**Figure 3** Evolution of the ratio of radius of gyration  $R_g$  of lysozyme at a given dose with respect to the initial value  $R_{g0}$  (first frame),  $R_g/R_{g0}$ , with absorbed dose, in the presence of different additives. Samples of  $7.2 \text{ mg ml}^{-1}$  lysozyme were analysed in 40 mM sodium acetate, pH 3.8, 150 mM sodium chloride. Multiple frames of 0.035 s exposure time were recorded and added per point. Measurements were performed in the presence of 2 mM DTT, 5% v/v glycerol, 1 mM ascorbic acid and increasing concentrations of uridine (5, 10, 15, 20, 40, 100 mM). Samples without any additive were also analysed as negative controls. All the samples were measured in static mode (DTT: dithiothreitol; Asc: ascorbic acid; Glyc: glycerol; U: uridine).

In order to assess the quality of the SAXS data in static mode from lysozyme obtained in the presence of 100 mM uridine, frames below the critical dose that are statistically similar were averaged, and  $R_g$  calculated using two methods: the Guinier approximation and the pair-distance distribution function  $P(r)$ . The maximum particle dimension  $D_{\text{max}}$ , was also determined from the  $P(r)$  function. Calculation of  $R_g$  and  $D_{\text{max}}$ , as well as *ab initio* modelling, was performed by using 20 frames out of 76 lying below the critical dose threshold. The frames, which have an accumulated dose of 3.8 kGy, were selected using *CorMap* (Franke *et al.*, 2015). For comparison, the scattering profile of lysozyme in flow mode in the absence of uridine was also collected (Fig. 5). In this case, only two frames were statistically similar, according to

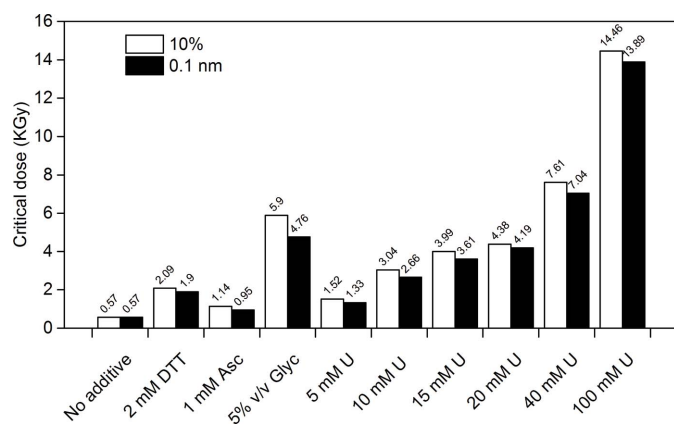


**Figure 4**  
Critical doses determined using two different metrics for lysozyme  $7.2 \text{ mg ml}^{-1}$  in the presence and absence of different additives to limit radiation damage. White columns: critical dose defined as the dose where the increase in  $R_g$  is maximum 10%. Black columns: critical dose specified as the dose required to change  $R_g$  by a maximum of 0.1 nm relative to the initial data frame, as defined by Jeffries *et al.* (2015). All samples were measured in static mode (DTT: dithiothreitol; Asc: ascorbic acid; Glyc: glycerol; U: uridine).

*CorMap*, and could be used to calculate  $R_g$ . The selected 20 frames in static mode with 100 mM uridine and the two frames in flow mode without uridine show similar SAXS profiles, typical of scattering curves from a globular protein in solution. Interestingly, the presence of 100 mM uridine does not affect the intensity of the scattering profile. The  $R_g$  values calculated with the Guinier approximation were  $1.45 \pm 0.03 \text{ nm}$  and  $1.46 \pm 0.04 \text{ nm}$  for the control sample and that containing 100 mM uridine, respectively. Moreover, the experimental SAXS profile of lysozyme in the presence of 100 mM uridine fits well with the theoretical scattering profile predicted from the crystal structure ( $\chi^2 = 0.98$ ) (Fig. 5a). The superposition of the profile collected in flow mode is also shown for comparison ( $\chi^2 = 1.08$ ) (Fig. 5b).

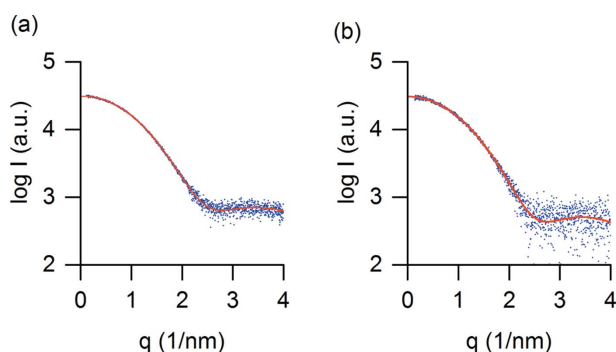


**Figure 5**  
Fitting of the experimental SAXS data (blue dots) with the theoretical scattering curve predicted from the crystal structure (PDB ID 4n8z, red line) for (a) lysozyme collected in static mode in the presence of 100 mM uridine ( $\chi^2 = 0.98$ ) and (b) lysozyme without any additive collected by flowing the sample while exposed to the beam ( $\chi^2 = 1.08$ ). Experimental data result from the averaging of the statistically similar frames below the critical dose validated by *CorMap* (Franke *et al.*, 2015) (20 frames for lysozyme with uridine in static mode and two frames for lysozyme without additive in flow mode).

**Table 2**

Analysis of the quality of the data from SAXS experiments on lysozyme in a solution with 100 mM uridine measured in static mode.

The structural parameters obtained from the  $P(r)$  function of lysozyme in 100 mM uridine are compared with those of the entry SASDA96 in the Small Angle Scattering Biological Data Bank (SASBDB) deposited by Franke *et al.* (2015).

Structural parameters	This study†	Franke <i>et al.</i> (2015)‡
Experimental $R_g/I_1$	1.45	1.51
$P(r)R_g/I_1$	1.45	1.51
Porod volume ( $\text{nm}^3$ )	21.0	24
$D_{\text{max}}$ (nm)	4.5	4.8

† 40 mM Sodium acetate, pH 3.8, 150 mM NaCl, 100 mM uridine. ‡ 20 mM Sodium acetate, 20 mM HEPES, pH 6.8, SASBDB ID SASDA96 (Franke *et al.*, 2015).

The  $P(r)$  distribution function for lysozyme in the presence of 100 mM uridine (Fig. 6) was used to calculate  $R_g$ ,  $D_{\text{max}}$  and the Porod volume. The values extracted are of the order of the values deposited at the Small-Angle Scattering Biological Data Bank (<http://www.sasbdb.org>) by Valentini *et al.* (2015) and by Franke *et al.* (2015) (Table 2). Twenty *ab initio* dummy atom models of lysozyme were obtained from the scattering patterns. The most probable model has a normalized spatial discrepancy (NSD) with respect to the rest of the set of 0.499, which indicates good stability in the solution (Kozin & Svergun, 2001). The model is shown in Figure S4 of the supporting information aligned with the high-resolution crystallographic structure.

#### 4. Discussion

The significant global metrics consistently show an increasing scavenging effect of uridine as its concentration is increased in lysozyme crystals at room temperature. The enhancement factors  $D_{1/2,U}/D_{1/2}$  and  $S_{AD,U}/S_{AD}$  for 1 M uridine are 1.76 and 0.37, respectively. These values are comparable with the factors achieved by other scavengers previously reported for

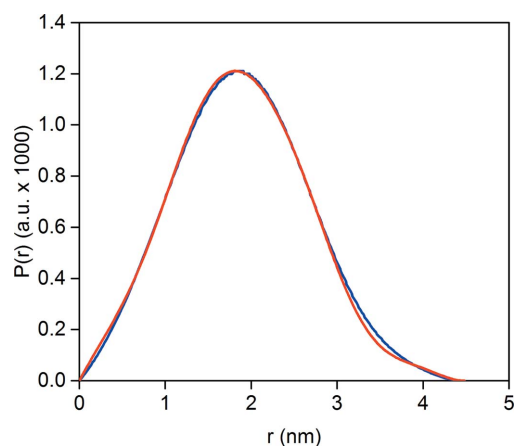


**Figure 6**  
Pair-distance distribution functions  $P(r)$  derived from the Fourier transform of the scattering profile of lysozyme in the presence of 100 mM uridine without flowing the sample (blue curve) and lysozyme without any additive, collected by flowing the sample while exposed to the beam (red curve).

lysozyme crystals at room temperature, namely ascorbate at 0.5 M minimum [factor 2 in  $D_{1/2,U}/D_{1/2}$  (Barker *et al.*, 2009)] and sodium nitrate at 0.1 M [factor 0.47 in  $S_{AD,SodiumNitrate}/S_{AD}$  (Kmetko *et al.*, 2011)]. These irradiation experiments are comparable in spite of the different protocols, variability of the crystals and the diverse X-ray beam properties, as shown by the obtained values of  $D_{1/2}$ . The value for  $D_{1/2}$  obtained by Barker *et al.* is 0.9 MGy at a dose rate of 2.8 kGy s<sup>-1</sup>, which is in good agreement with our results of 1.06 and 1.11 MGy obtained at 13.8 and 20.0 kGy s<sup>-1</sup>, respectively. The values of  $D_{1/2}$  are consistent with the observation made by Warkentin *et al.* (2012) on thaumatin crystals that radiation damage is not dependent on the absorbed dose rate at room temperature at the typical irradiation levels achievable at synchrotron beamlines. It is worth noting that the value of  $S_{AD}$  reported by Kmetko *et al.* (2011) for control native lysozyme crystals at room temperature, 0.57 Å<sup>2</sup> MGy<sup>-1</sup>, differs from the values 0.115 and 0.191 Å<sup>2</sup> MGy<sup>-1</sup> obtained here at 13.8 and 20.0 kGy s<sup>-1</sup>, respectively. The discrepancy may be explained by the differences in the experimental set up. Moreover, the use of  $S_{AD}$  at room temperature suffers from the lack of linearity of the relative increase of the  $B$ -factors with respect of the absorbed dose (Fig. 1c). On the contrary, the use of  $S_{AD}$  at 100 K is justified as  $B$ -factors increase linearly at low doses (Kmetko *et al.*, 2006). To better fit the evolution of the  $B$ -factors with dose at room temperature, we have assumed an exponential increase of the  $B$ -factor with dose, that is

$$\Delta B = B_0[\exp(k\Delta D) - 1], \quad (2)$$

where  $B_0$  is the  $B$ -factor at close-to-zero dose,  $\Delta D$  is the differential dose within data sets, and  $k$  is the sensitivity of the  $B$ -factors to the dose. This equation reduces to the standard linear fit at low doses or low sensitivities, *i.e.*

$$\Delta B \simeq kB_0\Delta D, \quad (3)$$

as used for data sets collected at 100 K. Results using an exponential fit and its linear approximation at low doses for data sets collected at room temperature are shown in Table 1.

Lysozyme does not show significant specific radiation damage at room temperature (Figure S2 in the supporting information). Only some differential electron density in residue Met105 and in three out of four disulfide bonds was barely noticeable in difference maps ( $F_{obs,2} - F_{obs,1}$ ,  $\alpha_{calc,1}$ ) contoured at  $-4\sigma$  (Fig. 2). Conversely, global damage in MX experiments at room temperature is much more apparent, as seen comparing the effects in Figs. 1 and 2, respectively.

In SAXS experiments, lysozyme dissolved in a buffer containing uridine consistently shows a higher critical dose than the control. The critical dose of lysozyme in a solution without additives is 0.57 kGy, whereas in solution containing uridine the critical dose increases with concentration close to linear up to 14.46 kGy at 100 mM uridine (Fig. 4). Uridine is therefore acting as a scavenger and is able to prevent aggregation at high radiation dose. Indeed, uridine at 40 mM concentration is as efficient as 5% *v/v* glycerol (679 mM) in limiting radiation-induced aggregation of lysozyme, and shows a higher critical dose than 2 mM DTT or 1 mM ascorbic acid.

**Table 3**

Comparison of the critical doses reported for lysozyme in the presence of additives to limit radiation damage.

The critical doses calculated in this work by using two different metrics are compared with those reported in the literature (Jeffries *et al.*, 2015; Kuwamoto *et al.*, 2004). All the samples in these studies were measured in static mode.

Additive	This study (10%) <sup>†</sup>	This study (0.1 nm) <sup>‡</sup>	Jeffries <i>et al.</i>	Kuwamoto <i>et al.</i>
No additive	0.57 kGy	0.57 kGy	0.37 kGy	0.4 kGy
DTT	2.09 kGy <sup>§</sup>	1.90 kGy <sup>§</sup>	1.1 kGy <sup>¶</sup>	Not analyzed
1 mM Ascorbic acid	1.14 kGy	0.95 kGy	1.1 kGy	Not analyzed
5% Glycerol	5.90 kGy	4.57 kGy	2.6 kGy	Not observed <sup>††</sup>

<sup>†</sup> 10% Criteria: critical dose is the dose at which  $R_g$  increases by 10% maximum with respect to the value of  $R_g$  in first data frame. <sup>‡</sup> 0.1 nm Criteria: critical dose is the dose at which  $R_g$  increases by 0.1 nm maximum with respect to the initial value of  $R_g$ . <sup>§</sup> 2 mM DTT. <sup>¶</sup> 1 mM DTT. <sup>††</sup> No radiation damage observed at a total accumulated dose of 2 kGy.

A concentration as low as 10 mM uridine is still more effective as a scavenger than DTT or ascorbic acid at the tested concentrations. Our results also confirm that glycerol is more effective than DTT or ascorbic acid in limiting radiation damage on lysozyme, as reported by Jeffries *et al.* (2015).

The values of the critical dose for lysozyme in solution without additives and in the presence of glycerol, DTT and ascorbic acid are close to those reported by Kuwamoto *et al.* (2004) and Jeffries *et al.* (2015) (Table 3). The factor of two difference in the critical dose for the DTT value is probably due to the different concentration of DTT that we have used (2 mM) compared here with that used by Jeffries *et al.* (1 mM). The differences in the observed critical doses, in all cases less than a factor two, could be due to the different dose rate between experiments or differences in protein concentration, as it has previously been reported that these factors influence the critical dose (Kuwamoto *et al.*, 2004) (Table S4 in the supporting information). The experiments reported here were performed at 7.2 mg ml<sup>-1</sup> lysozyme, while experiments reported by Kuwamoto *et al.* (2004) and Jeffries *et al.* (2015) were performed at 4.9 mg ml<sup>-1</sup> and 8.8 mg ml<sup>-1</sup>, respectively. The choice of the metrics does not significantly influence the critical dose, as values calculated using the two different metrics show similar trends and similar values within 20% (Fig. 4, Table 3).

Structural data support the conclusion that uridine protects lysozyme from the attack of the ROS, at least up to 3.8 kGy absorbed dose in a solution containing 100 mM uridine. The lysozyme crystal structure agrees well with the scattering profile (Fig. 5). The pair-distance distribution function  $P(r)$  is typical for a globular protein such as lysozyme and overlays well with the control sample  $P(r)$  (Fig. 6). Also, the *ab initio* shape reconstruction superimposes well onto the crystal structure (Fig. S4 in the supporting information). The maximal dose of 3.8 kGy absorbed by lysozyme in a solution containing uridine can be compared with the maximal dose of 0.57 kGy that could be used to obtain similar structural data for lysozyme without this additive. These results indicate that the useful data range increases by a factor of seven when adding 100 mM uridine in the solution. This may open the door to

study some systems in static mode rather than flow mode, which translates to lower sample consumption. Uridine does not affect the stability of lysozyme, as checked by determining the structure of the protein at low resolution. Furthermore, uridine is soluble at concentrations as high as 2 M.

Although showing similar efficiency in SAXS experiments, uridine and glycerol limit radiation damage of lysozyme in solution through different mechanisms. Glycerol interacts with hydroxyl radicals and prevents the association of proteins containing amino acid side-chain modifications produced by ROS and solvated electrons (Kuwamoto *et al.*, 2004). On the other hand, uridine has been described to react with hydroxyl and hydrogen radicals, and with solvated electrons (Greenstock *et al.*, 1969). Unlike glycerol, there is no evidence that uridine affects protein–protein interactions.

An advantage of uridine with respect to glycerol is its lower viscosity, which eases the pipetting of solutions and facilitates the preparation of accurate ‘matching buffers’. Also, uridine appears to be less prone to cause effects on protein–protein and protein–solvent interactions than glycerol, which may induce a shift to a more compact conformation of the protein, inducing these unexpected effects (Vagenende *et al.*, 2009). However, uridine should be employed with caution in RNA binding proteins, as well as proteins binding ligands containing nucleotide moieties.

## 5. Conclusions

This study demonstrates the beneficial properties of uridine for the acquisition of high-quality MX and SAXS datasets at room temperature adding uridine to the list of available scavengers. A portfolio of scavengers is needed since the approach to reduce damage by X-rays at synchrotron light sources must be tailored to each protein target in order to obtain high signal-to-noise ratio without altering the structure of the macromolecule. Furthermore, for complementary experiments, being able to use the same scavenger for different techniques could decrease potential sources of uncertainty.

Specifically for MX studies, uridine has been shown to reduce the global effects of radiation damage on crystals at room temperature. The scavenging effect is proportional to the concentration of uridine up to 1 M, when the critical dose is increased by ~70% and *B*-factors decrease by ~40% with respect to the same crystal without the addition of uridine. It is worth noting that the evolution of the *B*-factors with dose at room temperature was well fitted using an exponential curve, and that the sensitivity was defined as the slope of the equivalent linear regression. Uridine was not shown to protect specific residues, even those reported as being more sensitive to radiation damage (Cys, Asp, Glu). Furthermore, no scavenging effects due to uridine were observed in cryoprotected crystals at 100 K. Our data support the view that radiation damage at room temperature is not dependent on the dose rate for the range studied here (13.8 and 20 kGy s<sup>-1</sup>), except at high doses (above 1.2 MGy), when the crystals appear to be slightly less radiation sensitive. Finally, we note

that the crystallographic structure of a lysozyme crystal soaked into a 1 M uridine solution was identical to the structure obtained without uridine.

Concerning the SAXS experiments, the results presented here demonstrate that uridine can be considered as a suitable scavenger at room temperature, for concentrations ranging between 5 and 100 mM. Uridine at concentrations between 20 and 40 mM has the same scavenging effect as 679 mM (5% *v/v*) glycerol, which in turn has been described to be more effective than DTT or ascorbic acid (Jeffries *et al.*, 2015). We show that 100 mM uridine provides high-quality data up to an absorbed dose of 3.8 kGy. Uridine was also shown not to affect the structure of the protein up to concentrations of 100 mM. In addition to good scavenging properties, uridine is highly soluble in water and does not increase the background significantly with respect to the control solution without the additive. The use of uridine is particularly appropriate for SAXS experiments with small sample volumes, as it allows the collection of more data frames in static mode before significant radiation damage develops.

## Acknowledgements

This work was supported by the Spanish Nuclear Safety Council (Consejo de Seguridad Nuclear, CSN). Access to the P12 BioSAXS beamline at Petra III (DESY, Hamburg) was facilitated by the European Community’s Seventh Framework Programme (FP7/2007–2013) under BioStruct-X (grant agreement N°283570). We thank Dmitri Svergun and co-workers from EMBL-Hamburg for their support and collaboration. The authors also thank Professor Arwen R. Pearson and Professor Elspeth Garman for useful discussions.

## References

- Allan, E. G., Kander, M. C., Carmichael, I. & Garman, E. F. (2013). *J. Synchrotron Rad.* **20**, 23–36.
- Barker, A. I., Southworth-Davies, R. J., Paithankar, K. S., Carmichael, I. & Garman, E. F. (2009). *J. Synchrotron Rad.* **16**, 205–216.
- Barty, A., Caleman, C., Aquila, A., Timneanu, N., Lomb, L., White, T., Andreasson, J., Arnlund, D., Bajt, S., Barends, T. R. M., Barthelmess, M., Bogan, M. J., Bostedt, C., Bozek, J. D., Coffee, R., Coppola, N., Davidsson, J., DePonte, D. P., Doak, R. B., Ekeberg, T., Elser, V., Epp, S. W., Erk, B., Fleckenstein, H., Foucar, L., Fromme, P., Graafsma, H., Gumprecht, L., Hajdu, J., Hampton, C. Y., Hartmann, R., Hartmann, R., Hauser, G., Hirsemann, H., Holl, P., Hunter, M. S., Johansson, L., Kassemeyer, S., Kimmel, N., Kirian, R. A., Liang, M., Maia, F. R. N. C., Malmerberg, E., Marchesini, S., Martin, A. V., Nass, K., Neutze, R., Reich, C., Rolles, D., Rudek, B., Rudenko, A., Scott, H., Schlichting, I., Schulz, J., Seibert, M. M., Shoeman, R. L., Sierra, R. G., Soltau, H., Spence, J. C. H., Stellato, F., Stern, S., Strüder, L., Ullrich, J., Wang, X., Weidenspointner, G., Weierstall, U., Wunderer, C. B. & Chapman, H. N. (2012). *Nat. Photon.* **6**, 35–40.
- Blanchet, C. E., Spilotros, A., Schwemmer, F., Graewert, M. A., Kikhney, A., Jeffries, C. M., Franke, D., Mark, D., Zengerle, R., Cipriani, F., Fiedler, S., Roessle, M. & Svergun, D. I. (2015). *J. Appl. Cryst.* **48**, 431–443.
- Daly, M. J. (2012). *DNA Repair (Amst.)*, **11**, 12–21.

- Daly, M. J., Gaidamakova, E. K., Matrosova, V. Y., Kiang, J. G., Fukumoto, R., Lee, D. Y., Wehr, N. B., Viteri, G. A., Berlett, B. S. & Levine, R. L. (2010). *PLoS One*, **5**, e12570.
- De la Mora, E., Carmichael, I. & Garman, E. F. (2011). *J. Synchrotron Rad.* **18**, 346–357.
- Diederichs, K. (2006). *Acta Cryst.* **D62**, 96–101.
- Dong, J., Boggon, T. J., Chayen, N. E., Raftery, J., Bi, R.-C. & Helliwell, J. R. (1999). *Acta Cryst.* **D55**, 745–752.
- Emsley, P., Lohkamp, B., Scott, W. G. & Cowtan, K. (2010). *Acta Cryst.* **D66**, 486–501.
- Evans, P. (2006). *Acta Cryst.* **D62**, 72–82.
- Fischetti, R. F., Rodi, D. J., Mirza, A., Irving, T. C., Kondrashkina, E. & Makowski, L. (2003). *J. Synchrotron Rad.* **10**, 398–404.
- Flot, D., Mairs, T., Giraud, T., Guijarro, M., Lesourd, M., Rey, V., van Brussel, D., Morawe, C., Borel, C., Hignette, O., Chavanne, J., Nurizzo, D., McSweeney, S. & Mitchell, E. (2010). *J. Synchrotron Rad.* **17**, 107–118.
- Franke, D., Jeffries, C. M. & Svergun, D. I. (2015). *Nat. Methods*, **12**, 419–422.
- Franke, D. & Svergun, D. I. (2009). *J. Appl. Cryst.* **42**, 342–346.
- French, S. & Wilson, K. (1978). *Acta Cryst.* **A34**, 517–525.
- Garman, E. F. (2010). *Acta Cryst.* **D66**, 339–351.
- Garman, E. F. & Weik, M. (2011). *J. Synchrotron Rad.* **18**, 313–317.
- Garrison, W. M. (1987). *Chem. Rev.* **87**, 381–398.
- Gerstel, M., Deane, C. M. & Garman, E. F. (2015). *J. Synchrotron Rad.* **22**, 201–212.
- Greenstock, C. L., Hunt, J. W. & Ng, M. (1969). *Trans. Faraday Soc.* **65**, 3279–3287.
- Grishaev, A. (2012). *Curr. Protoc. Protein Sci.* **70**, 17.14.1–17.14.18.
- Guinier, A. (1939). *Ann. Phys.* **12**, 161–237.
- Hammel, M., Kriechbaum, M., Gries, A., Kostner, G. M., Laggner, P. & Prassl, R. (2002). *J. Mol. Biol.* **321**, 85–97.
- Henke, B. L., Gullikson, E. M. & Davis, J. C. (1993). *At. Data Nucl. Data Tables*, **54**, 181–342.
- Holton, J. M. (2009). *J. Synchrotron Rad.* **16**, 133–142.
- Hong, X. & Hao, Q. (2009). *Rev. Sci. Instrum.* **80**, 014303.
- Howell, P. L. & Smith, G. D. (1992). *J. Appl. Cryst.* **25**, 81–86.
- Hura, G. L., Menon, A. L., Hammel, M., Rambo, R. P., Poole, F. L. II, Tsutakawa, S. E., Jenney, F. E. Jr, Classen, S., Frankel, K. A., Hopkins, R. C., Yang, S. J., Scott, J. W., Dillard, B. D., Adams, M. W. W. & Tainer, J. A. (2009). *Nat. Methods*, **6**, 606–612.
- Jacques, D. A. & Trehwella, J. (2010). *Protein Sci.* **19**, 642–657.
- Jeffries, C. M., Graewert, M. A., Svergun, D. I. & Blanchet, C. E. (2015). *J. Synchrotron Rad.* **22**, 273–279.
- Juanhuix, J., Gil-Ortiz, F., Cuní, G., Colldelram, C., Nicolás, J., Lidón, J., Boter, E., Ruget, C., Ferrer, S. & Benach, J. (2014). *J. Synchrotron Rad.* **21**, 679–689.
- Kabsch, W. (2010). *Acta Cryst.* **D66**, 125–132.
- Kmetko, J., Husseini, N. S., Naides, M., Kalinin, Y. & Thorne, R. E. (2006). *Acta Cryst.* **D62**, 1030–1038.
- Kmetko, J., Warkentin, M., English, U. & Thorne, R. E. (2011). *Acta Cryst.* **D67**, 881–893.
- Konarev, P. V., Volkov, V. V., Sokolova, A. V., Koch, M. H. J. & Svergun, D. I. (2003). *J. Appl. Cryst.* **36**, 1277–1282.
- Kozin, M. B. & Svergun, D. I. (2001). *J. Appl. Cryst.* **34**, 33–41.
- Kuwamoto, S., Akiyama, S. & Fujisawa, T. (2004). *J. Synchrotron Rad.* **11**, 462–468.
- Maleknia, S. D., Ralston, C. Y., Brenowitz, M. D., Downard, K. M. & Chance, M. R. (2001). *Anal. Biochem.* **289**, 103–115.
- Martel, A., Liu, P., Weiss, T. M., Niebuhr, M. & Tsuruta, H. (2012). *J. Synchrotron Rad.* **19**, 431–434.
- Meisburger, S. P., Warkentin, M., Chen, H., Hopkins, J. B., Gillilan, R. E., Pollack, L. & Thorne, R. E. (2013). *Biophys. J.* **104**, 227–236.
- Murray, J. W., Rudiño-Piñera, E., Owen, R. L., Gringer, M., Ravelli, R. B. G. & Garman, E. F. (2005). *J. Synchrotron Rad.* **12**, 268–275.
- Murshudov, G. N., Vagin, A. A. & Dodson, E. J. (1997). *Acta Cryst.* **D53**, 240–255.
- Nielsen, S. S., Møller, M. & Gillilan, R. E. (2012). *J. Appl. Cryst.* **45**, 213–223.
- Pernot, P., Round, A., Barrett, R., De Maria Antolinos, A., Gobbo, A., Gordon, E., Huet, J., Kieffer, J., Lentini, M., Mattenet, M., Morawe, C., Mueller-Dieckmann, C., Ohlsson, S., Schmid, W., Surr, J., Theveneau, P., Zerrad, L. & McSweeney, S. (2013). *J. Synchrotron Rad.* **20**, 660–664.
- Petoukhov, M. V., Franke, D., Shkumatov, A. V., Tria, G., Kikhney, A. G., Gajda, M., Gorba, C., Mertens, H. D. T., Konarev, P. V. & Svergun, D. I. (2012). *J. Appl. Cryst.* **45**, 342–350.
- Rajendran, C., Dworkowski, F. S. N., Wang, M. & Schulze-Briese, C. (2011). *J. Synchrotron Rad.* **18**, 318–328.
- Round, A., Felisaz, F., Fodinger, L., Gobbo, A., Huet, J., Villard, C., Blanchet, C. E., Pernot, P., McSweeney, S., Roessle, M., Svergun, D. I. & Cipriani, F. (2015). *Acta Cryst.* **D71**, 67–75.
- Schulze-Briese, C., Wagner, A., Tomizaki, T. & Oetiker, M. (2005). *J. Synchrotron Rad.* **12**, 261–267.
- Slade, D. & Radman, M. (2011). *Microbiol. Mol. Biol. Rev.* **75**, 133–191.
- Southworth-Davies, R. J., Medina, M. A., Carmichael, I. & Garman, E. F. (2007). *Structure*, **15**, 1531–1541.
- Svergun, D. I. (1992). *J. Appl. Cryst.* **25**, 495–503.
- Svergun, D., Barberato, C. & Koch, M. H. J. (1995). *J. Appl. Cryst.* **28**, 768–773.
- Svergun, D. I., Koch, M. H. J., Timmins, P. A. & May, R. P. (2013). *Small Angle X-ray and Neutron Scattering from Solutions of Biological Macromolecules*, IUCr Texts on Crystallography, Vol. 19. Oxford University Press.
- Vagenende, V., Yap, M. G. S. & Trout, B. L. (2009). *Biochemistry*, **48**, 11084–11096.
- Valentini, E., Kikhney, A. G., Previtali, G., Jeffries, C. M. & Svergun, D. I. (2015). *Nucleic Acids Res.* **43**, D357–D363.
- Warkentin, M., Badeau, R., Hopkins, J. B., Mulichak, A. M., Keefe, L. J. & Thorne, R. E. (2012). *Acta Cryst.* **D68**, 124–133.
- Winn, M. D., Ballard, C. C., Cowtan, K. D., Dodson, E. J., Emsley, P., Evans, P. R., Keegan, R. M., Krissinel, E. B., Leslie, A. G. W., McCoy, A., McNicholas, S. J., Murshudov, G. N., Pannu, N. S., Potterton, E. A., Powell, H. R., Read, R. J., Vagin, A. & Wilson, K. S. (2011). *Acta Cryst.* **D67**, 235–242.
- Yin, X., Scalia, A., Leroy, L., Cuttitta, C. M., Polizzo, G. M., Ericson, D. L., Roessler, C. G., Campos, O., Ma, M. Y., Agarwal, R., Jackimowicz, R., Allaire, M., Orville, A. M., Sweet, R. M. & Soares, A. S. (2014). *Acta Cryst.* **D70**, 1177–1189.
- Zeldin, O. B., Gerstel, M. & Garman, E. F. (2013). *J. Appl. Cryst.* **46**, 1225–1230.